Engineering Transactions, **66**(4): 427–442, 2018, doi: 10.24423/EngTrans.850.20181017
Polish Academy of Sciences • Institute of Fundamental Technological Research (IPPT PAN)
Université de Lorraine • Poznan University of Technology

Research Paper

Experimental Verification of the Steering Performance of All-Hydraulic Crawler Chassis

Xiaolian LV[1,2)], Xiaorong LV[3)*], Xiaojie SHI[2)], Tingyu WANG[3)]

[1)] *Key Laboratory of Modern Agricultural Equipment*
Ministry of Agriculture
Nanjing, Jiangshu, 210014, China

[2)] *College of Machinery and Automotive Engineering*
Chuzhou University
Chuzhou, Anhui, 239000, China

[3)] *College of Machinery & Electronics*
Sichuan Agricultural University
Ya'an, Sichuan, 625014, China
[*]e-mail: lxrxj2008@163.com

The force conditions in the steering system of the chassis under different conditions are analyzed theoretically for the independently designed and developed all-hydraulic crawler chassis. Using the multi-body dynamic simulation software RecurDyn, the chassis steering performance on sandy loam and clay pavements, and the steering performance under different steering radiuses on the sandy loam pavement are simulated and analysed dynamically respectively. The steering resistance moment is studied when the pavement conditions and steering radius are different. This research selects inside and outside crawler slip ratio as an index, and road conditions, speed and steering radius as factors to test the steering performance of all-hydraulic crawler chassis under different operating conditions. It is observed from the simulation results that during the pivot steering on the sandy loam, the drive torque and braking torque of the driving wheel are larger than on the clay ground. With the decrease of the steering radius, the torques of the left and right driving wheel are both gradually increasing. In the same steering radius, the torque of the outside driving wheel is larger than that of the inside driving wheel. The simulation results are consistent with the theoretical analysis results. In the steering performance test, the factors influencing the slippage rate on both sides of the crawler are such that the influence of the steering radius is greater than that pf the pavement condition and the pavement condition influence is greater than that of the speed. Among them, the steering radius has a significant influence on the slip ratio of the inside crawler, and an extremely significant influence on the slip ratio of the outside crawler. This research can provide a certain theoretical basis and technical reference for the development of hydraulic crawler chassis and optimization of the steering system.

Key words: crawler chassis; steering; dynamics simulation; RecurDyn; performance test.

1. Introduction

Crawler chassis provides good terrain grip and wide traction and is suitable for a heavy load. It can be used in wet and muddy terrain or difficult terrain. Due to its low grounding pressure, good compaction and light environmental damage to the farmland, it is suitable for the traction work on mountains and foothills [1]. Steering performance is an important indicator of the crawler chassis mobility, whether the steering is flexible or not would directly affect the application effect of the chassis, the fuel economy and the driver's labor intensity. Until now, several studies on tracked vehicles have been conducted [2–9]. Chi *et al.* performed tracked prototype experiments on soft terrain, next they studied the relationships between steering power ratio and turning radius, skid ratio and steering coefficient, and proposed a new measuring method to reduce the experimental error of steering power ratio. Li *et al.* built 3-DOF dynamic models considering sideslip, yaw and roll of vehicle steering based on the Newton mechanics and Euler rigid body dynamics. They performed simulation and analysis of lateral velocity, sideslip angle, yaw rate, and roll rate in two different running conditions of low and high velocity for front-wheel steering and four-wheel steering. Yang *et al.* conducted the steering simulation by using MATLAB/Simulink and analyzed the steering process of a hydrostatic drive tracked vehicle. Al-Milli *et al.* presented an analytical approach to track-terrain modeling and a novel traversability prediction simulator for tracked vehicles conducting steady-state turning maneuvers on soft terrain. The adopted models were modified to provide a generalized analytical solution. Ding *et al.* proposed more general and high-fidelity models for terrain characterization to satisfy the high requirements of autonomous wheeled vehicles. Sandu *et al.* tested the influence of payload, ground speed, sand gradation/grain size and sand moisture content on contact patch pressure and tire sinkage.

Due to the relatively complex operating conditions of the crawler chassis and the limitation of research techniques, the previous researches usually referred to the steering on the assumed rigid pavement. In this paper, the main aim is to study the operating situation under different working conditions by using the developed steering dynamic system model obtained with simulation software. In recent years, with the development of ground mechanics and multi-body dynamics, such an approach has provided theoretical and technical support to solve the complex problems of crawler vehicle itself. The RecurDyn simulation software uses the relative coordinate equation of motion and completely recursive algorithm. This software is very suitable for solving large-scale and complex contact dynamics problems. Full three-dimensional modeling of the crawler system can be carried out at the same time. Different types of crawler systems and a full dynamic tracked vehicle model were developed, and their interactions with the soft

and hard terrain were analysed in [10–12]. This article is based on torque theory of crawler-ground adhesion and uses RecurDyn to establish a multi-body system dynamics model and road model of the crawler chassis. The steering resisting torques in different pavement conditions and steering radiuses are analysed, and steering performance is tested through the chassis experiment. The study provides a certain theoretical basis and technical reference for the optimization design of the all-hydraulic crawler chassis and its performance improvement.

2. Structure and operation principle

The designed all-hydraulic crawler chassis with full hydraulic structure can be mainly used for hilly mountains operation. The chassis consists of engine, all-hydraulic system, walking system, and control system, as shown in Fig. 1. In operation, the transfer case receives power from the engine; the transfer case transfers power to a double pump and a gear pump for rotation. The hydraulic control valve is used to adjust the hydraulic cylinder to implement contact with the ground in order to reach the operating position. When the two control handles are pulled at the same time, the counter clockwise rotation valve of the double pump is opened, which makes the travel motor to rotate and the crawler moves forward. Similarly, when the two control handles are pulled backward, the chassis reverses. When the two control handles are pulled to different places at the same time, the chassis achieves positive differential steering; when a handle is pulled the chassis achieves unilateral brake steering. When a handle is pulled forward, and the other is pulled backward, the chassis achieves reverse differential steering, which is a full 360° pivot steering. When the machine walks or turns

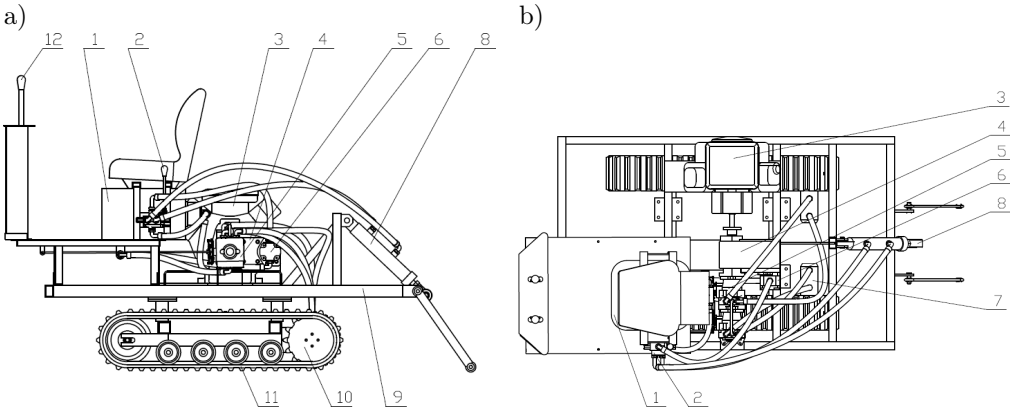

Fig. 1. Structure diagram of the chassis: a) front view, b) top view: 1 – tank, 2 – hydraulic cylinder control valve, 3 – engine, 4 – transfer case, 5 – double pump, 6 – gear pump, 7 – motor, 8 – hydraulic cylinder, 9 – chassis support seaming, 10 – driving system, 11 – crawler, 12 – control system.

on the road, it lifts the tool through the hydraulic cylinder for short-distance transport.

3. Force analysis in the chassis steering

Steering of the chassis is achieved through the speed difference on both sides; the size of speed difference determines o the size of the steering radius on different curved grounds. The crawler chassis steering under the simplified condition does not consider the inside and outside crawler on the ground, as it does not produce a slip. Due to the significant resistance incurred by the crawler vehicles during steering, they need to consume much more power in comparison to straight driving. Thereby, when the steering radius is different, the needed driving force of the inside and outside chassis is also different. This study focuses on the reverse differential steering, unilateral braking steering and positive differential stressing of the chassis for force analysis [13, 14].

3.1. The reverse differential steering

The crawlers on both sides are in the opposite driving state when the chassis is in reverse differential steering, and then the steering radius is $0 \leq R < B/2$. The stress force diagram of the chassis studied in this paper is shown in Fig. 2a for the initial steering ($R = 0$).

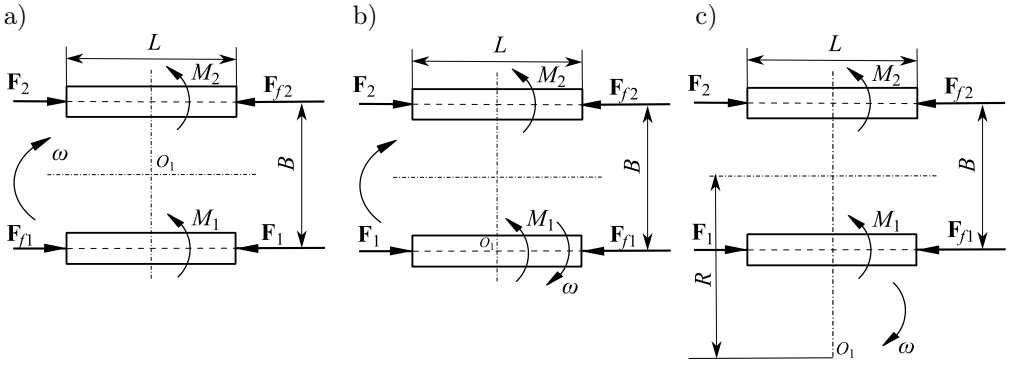

Fig. 2. Force analysis diagram of the chassis in different steering modes: a) the pivot steering, b) B/2 steering, c) the small radius steering.

In Fig. 2, O_1 is the steering center of the chassis, the outside crawler of the chassis is affected by driving force F_2 and friction force F_{f2}, and the inside track is affected by braking force F_1 and friction force F_{f1}. The steering radius is $R = \frac{B}{2}$. The steering resisting torque on both sides is $M_1 = M_2 = \frac{GL\mu}{8}$, where μ is the steering resistance coefficient. The outside track moves forward,

and the inside track moves backward to achieve reverse differential steering. By conducting force analysis on the chassis, the following formula can be obtained:

$$\begin{cases} F_2 + F_{f1} - F_1 - F_{f2} = 0, \\ (F_1 + F_2)\dfrac{B}{2} - (F_{f1} + F_{f2})\dfrac{B}{2} - M_1 - M_2 = 0. \end{cases} \tag{3.1}$$

From the conditions of the average steering, $F_{f1} = F_{f1} = 0.5F_f$ can be obtained and placed in Eq. (3.1). The driving force F_2 of the outside crawler is

$$F_2 = F_{f2} + \frac{2M_1}{B} = \frac{GF_f}{2} + \frac{GL\mu}{4B}. \tag{3.2}$$

In this case, the driving forces needed on both sides are equal. The analysis shows that when the steering radius $R = 0$, the crawler can achieve the on-center steering, and then the steering resisting torque coming from the crawler is at a maximum, which requires the motors on both sides to produce a larger driving force. The smaller turning radius reduces the area of chassis steering, which makes the chassis more flexible.

3.2. Unilateral braking steering

In the process of unilateral braking steering, the driving motor of inside crawler does not need to generate a power output. Only the outside crawler needs to generate output power to drive. The chassis force is shown in Fig. 2b. Assuming the crawler chassis makes steering around the center O_2 of the inside crawler, and therefore the inside does not have to generate a power output; thus, the rolling resistance F_{f1} is 0, driving force F_1 is 0 and steering resisting torque is $M_1 = M_2 = \frac{GL\mu}{8}$. It can be obtained by force analysis as

$$\begin{cases} F_2 + F_1 - F_{f_1} - F_{f_2} = 0, \\ (F_2 - F_{f_2})B - M_1 - M_2 = 0. \end{cases} \tag{3.3}$$

The driving force of the outside crawler is

$$F_2 = F_{f2} + \frac{M_1 + M_2}{B} = \frac{GF_f}{2} + \frac{GL\mu}{4B}. \tag{3.4}$$

3.3. The positive differential steering

When the chassis is in the positive differential steering, the crawlers on both sides are in driving in the same direction, and then the steering radius is $B/2 \leq R \leq 2B$. The crawlers on both sides make steering motion around the steering center point O_3. The chassis force is shown in Fig. 2c.

Making force analysis on the chassis, the following equation can be obtained:

$$F_1\left(R-\frac{B}{2}\right)+F_2\left(R+\frac{B}{2}\right)-F_{f_1}\left(R-\frac{B}{2}\right) - F_{f_2}\left(R+\frac{B}{2}\right)-M_1-M_2=0. \tag{3.5}$$

The driving force of the inside and outside crawlers can be obtained from the following formula:

$$F_2=F_1=F_{f2}+\frac{M_1+M_2}{B}=\frac{GF_f}{2}+\frac{GL\mu}{4B}. \tag{3.6}$$

3.4. Analysis results

Based on the above analysis, the size of $M_1=M_2=\frac{GL\mu}{8}$, $F_2=\frac{F_fG}{2}+\frac{\mu GL}{4B}$ and driving force F is proportional to the steering damping coefficient μ. According to the formula determined by $\mu=\frac{\mu_{\max}}{0.85+0.15\frac{R}{B}}$, $\mu_{\max}$ is the largest steering force coefficient when the crawler makes pivot steering. It can be concluded that μ is in inverse proportion with R, i.e., μ increases with the decrease of steering radius R; thus the driving force F also increases. Therefore, when the crawlers make pivot steering, the driving force and the steering resisting torque are at maximum.

4. The dynamics simulation of the steering system

In order to facilitate the analysis of the chassis, the following assumed conditions before the simulation model are established [15–17]:

1) the geometrical center and the gravity center of the chassis coincide;
2) the steering resistance coefficient $\mu=0.7$–0.85 and the steering resistance torque of the crawlers on both sides are equal;
3) by ignoring the effect of the internal resistance of the vehicle, the horizontal force forms the steering resistance torque with uniform distribution;
4) the body gravity distributed uniformly around the grounding length of the crawlers and the rolling resistance are equal;
5) as the grounding length of the crawlers is larger than the width of the crawler , the effect of the crawler width is not considered;
6) regardless of the soil shear and gradient resistance of soft terrain, the speed of crawler chassis steering is low, ignoring the effect of centrifugal force.

4.1. The establishment of dynamic model

4.1.1. The chassis model and motion constraints. In order to carry out simulation analysis, the UG software and the multi-body dynamics software RecurDyn/Track (LM) were used to complete the three-dimensional dynamics model of the chassis. The chassis is composed of chassis frame and crawler system. Each subsystem of the crawler is composed of all wheels and crawlers. First, the three-dimensional model of the body frame and hydraulic system are established by using the UG software, and exporting the completed model file in (*.stp) format; in order to reduce the simulation scale, the structure is simplified without affecting the accuracy of the analysis. Then, the *.stp format file is imported into the multi-body dynamic simulation software RecurDyn, and the three-dimensional model of each component of the low-speed crawler system is established by using the crawler subsystem Track/HM in the software; the virtual prototype model of tracked chassis is established by the assembly. Finally, according to the actual connection situation between the components of the chassis, the corresponding motion pair and load are added, and the relationships between the chassis and the ground as well as the pavement parameters are determined; the dynamics simulation model of the chassis is established.

4.1.2. The relationship between the chassis and the ground and the establishment of the pavement model. In view of different types of ground, the calculation of forces acting between the chassis and the ground is different. In the simulation analysis model, the pressure between crawler shoe and the ground uses crawler contact for definition. The pressure between crawler shoe and the soft ground uses contact force, which uses the shearing strength produced by the interaction between them to achieve. The computational formula of contact-impact force in RecurDyn is as follows [18]:

$$F = -k(q - q_0)^n - cq, \tag{4.1}$$

where F is the ground pressure, k is the stiffness coefficient, $q - q_0$ is the sinkage, q is the strain rate, c is the damping coefficient, and n is the deformation index of the soil.

In soft ground model, the soil has the function of "memory", namely loading history [7]. The positive pressure of crawler chassis on the ground is based on the pressure – subsidence relationship first put forward by M.G. Beck, the relation with loading is as follows:

$$P_{di} = \left[\frac{k_c}{b} + k_\varphi\right] \cdot z^n. \tag{4.2}$$

The relation with unloading is

$$P_{di} = P_{\max} - (K_0 + A_u Z_{\max})(Z_{\max} - Z), \tag{4.3}$$

where P_{di} is the ground pressure, k_c and k_φ are the soil cohesion and friction deformation modulus respectively, b is the depth of the crawler, z is the deformation depth, n is the deformation index of the soil, $Z_{\max}$ is the maximum deformation depth, $P_{\max}$ is the maximum pressure, K_0 and A_μ are the characteristic parameters of soil.

The calculation of forces acting between the crawler and the horizontal force of the ground is also based on Beck theory, the relation between shear stress and shear displacement is [7]

$$\tau(j, z) = (c + P_{di} \tan \varphi)(1 - \mathrm{e}^{-j/m}), \tag{4.4}$$

where τ is the shear stress, j is the shear displacement, φ is the angle of shearing resistance, and m is the shear deformation modulus.

The characteristic parameters of pavement used in steering simulation are shown in Table 1, and the steering simulation is shown in Fig. 3.

Table 1. Characteristic parameters of the pavement.

Parameter name	Sandy loam ground	Clay ground
Cohesive soil deformation modulus [$\mathrm{N{\cdot}m^{-(n+1)}}$]	$5.27{\cdot}10^{-3}$	$1.319{\cdot}10^{-2}$
Internal friction of the soil deformation modulus [$\mathrm{s{\cdot}m^{-(n+2)}}$]	1.151504	$6.9215{\cdot}10^{-1}$
Soil deformation index	0.7	0.5
Cohesion [Pa]	$1.27{\cdot}10^{-3}$	$4.14{\cdot}10^{-3}$
Shear resistance angle [$^\circ$]	29	13
Shear deformation modulus	25	25
Sinking rate	$5{\cdot}10^{-2}$	$5{\cdot}10^{-2}$

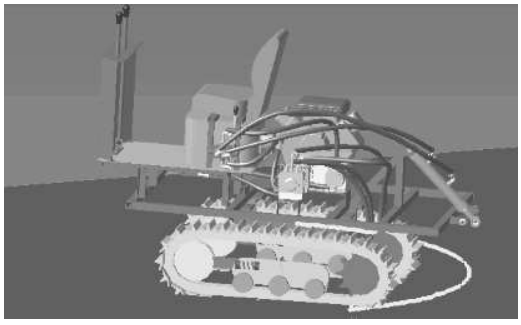

FIG. 3. Virtual steering simulation of the model.

4.2. Simulation results and analysis

4.2.1. The pivot steering simulation under different pavement conditions. To simulate pivot steering process, the hinge driving applied by the driver is the speed constraint function associated with the time. The cubic polynomial approximation STEP is to define a smooth step function [19], the function expression is as follows:

$$\begin{cases} \text{Outside: STEP (Time, } 1, 0, 3, -4.5), \\ \text{Inside: STEP (Time, } 1, 0, 3, 4.5). \end{cases}$$

where, in the first second, the speed of the vehicle is zero; under the effect of the gravity, the chassis is down to the pavement and reaches static balance. Within 1–3 second, the vehicle begins to accelerate, steering speed of the left driving wheel accelerates from zero to $\omega = 4.5$ rad/s, and the right driving wheel accelerates from zero to $\omega = 4.5$ rad/s reversely. The simulation time is 10 seconds, and the count is set to 250. The minus in the function expresses that the driving is in the opposite direction to the chassis movement. Pavement conditions with sandy loam and clay are simulated respectively, and the output results of the steering drive torque of the chassis driver under different pavement conditions are obtained, as shown in Fig. 4. The simulation results show that in the steering, in order to overcome the resistance torque produced by the soil and obtain enough driving torque, the driving torque of the outside driver needs to increase while the inside driver is impacting inversely the braking torque to achieve steering. The driving and braking torque of the driving wheel is larger than the pavement resistance when the crawler chassis is in the inverse differential steering on the sandy loam. That is because the outside resistance of the sandy loam pavement is larger than the clay. In the reverse differential steering, the friction resistance and bulldozing resistance on the sides between the chassis and the ground is increasing gradually, and the sinking of the chassis makes the soil shear force to increase. Therefore, in order to guarantee the driving, the stability in the steering, the driving torque and braking torque is needed to increase at the same time to meet the needs of normal steering.

4.2.2. Simulation on different steering radius of sandy loam pavement. In order to further research the influence of steering radius on the steering performance when the crawler chassis makes steering on the sandy loam pavement, the pavement condition is set as sandy loam ground. The same outside and different inside STEP function are set for loading. The simulation results of the clockwise steering under operating conditions on sandy loam are shown in Table 2.

a)

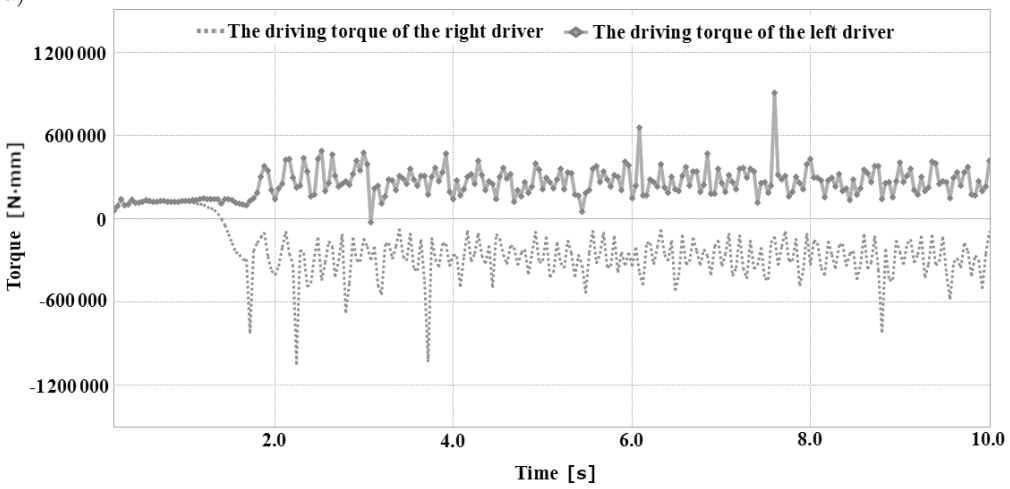

b)

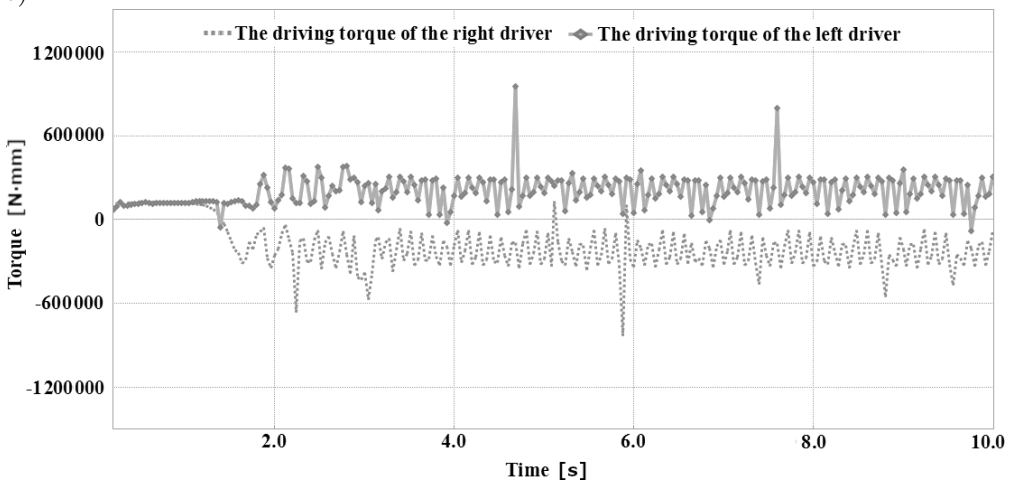

FIG. 4. The steering drive torque on different pavements: a) sandy loam pavement, b) clay pavement.

Table 2. Steering simulation results on the different steering radius on the sandy loam pavement.

Steering radius R [m]	Inside drive wheel torque M_I [N · m]	Outside drive wheel torque M_{II} [N · m]
∞ (driving straight)	170.053	177.831
$R > B/2$ (positive differential steering)	215.361	465.284
$R = B/2$ (unilateral braking)	435.322	495.825
0 (pivot steering)	547.689	556.261

The simulation result shows that the left and right driving wheel torque increases gradually with a decrease of the steering radius. In the same steering radius, the outside driving wheel torque is larger than the inside driving wheel torque. The maximum driving wheel torque appears at the pivot steering (steering radius $R = 0$), and then the inside and outside driving wheel torques are roughly equal to approx. 552 N · m. The resistance torque of the pivot steering is far higher than the unilateral braking steering, and the operation of the resistance torque for the pivot steering is flexible. Seven seconds are needed for the steering body to rotate 360°. Therefore, the short steering time can improve work efficiency and the steering covers a small area. The simulation results are consistent with the theoretical calculation and analysis results.

5. Performance test for the steering system

5.1. Test equipment and methods

In the test, the in-house developed full hydraulic crawler chassis is used, and its steering performance under the different conditions is tested. The inside crawler slip ratio δ_Y [%] and the outside crawler slip ratio δ_Z [%] are selected as indexes [20–22]. Pavement condition A, speed B and steering radius C are chosen as factors, the factor level of steering test is shown in Table 3. In the test, the actual steering radius of the chassis and the time of chassis making a full circle are tested. Due to different rotating circles on both sides of the chassis, the circles of the driving wheels on both sides after the chassis rotates a cycle are calculated respectively.

Table 3. The level of factor list of the steering test.

Level	Pavement condition A [%RH]	Speed B [m/s]	Steering radius C [m]
1	Dry cement pavement	0.48	0 (pivot steering)
2	Relative humidity of the field 40	0.70	0.36 (unilateral steering)
3	Relative humidity of the field 60	1.06	1.50 (free steering)

The calculation formula of the slip ratio is as follows:

$$\delta_y = \left[1 - \frac{S_{e1}}{2\pi r \cdot K_1}\right] \cdot 100\% = \left[1 - \frac{2\pi R_1}{2\pi R \cdot K_1}\right] \cdot 100\% = \left[1 - \frac{R_1}{r \cdot K_1}\right] \cdot 100\%, \tag{5.1}$$

$$\delta_z = \left[1 - \frac{S_{e2}}{2\pi r \cdot K_2}\right] \cdot 100\% = \left[1 - \frac{2\pi R_2}{2\pi R \cdot K_2}\right] \cdot 100\% = \left[1 - \frac{R_2}{r \cdot K_2}\right] \cdot 100\%, \tag{5.2}$$

where S_{e1} and S_{e2} are the routes of inside and outside crawler moving, K_1 and K_2 are the circles of inside and outside crawler rotating, and R_1 and R_2 are the actual steering radiuses of inside and outside crawler.

5.2. Test results and analysis

The results of the range analysis of the steering performance of the chassis are shown in Table 4. The results of the analysis of the variance in the conducted tests are shown in Table 5, where the effects of different operating conditions on steering performance of the chassis are also shown.

Table 4. The test results of the range analysis of the steering performance.

Test No.	Factors				Test index	
	Pavement condition A	Speed B	Steering radius C	Empty column	Outside crawler slip ratio δ_Z	Inside crawler slip ratio δ_Y
1	1	1	1	1	9.11	4.46
2	1	2	2	2	−16.40	38.54
3	1	3	3	3	−29.82	31.09
4	2	1	2	3	−22.22	37.48
5	2	2	3	1	−23.64	29.65
6	2	3	1	2	5.05	−1.44
7	3	1	3	2	−29.82	24.79
8	3	2	1	3	−2.26	1.80
9	3	3	2	1	−22.22	32.75
K_{Y1j}	−37.11	−42.93	11.90	−36.75		
K_{Y2j}	−40.81	−42.30	−60.84	−41.17		
K_{Y3j}	−54.30	−46.99	−83.28	−54.30		
$\overline{K_{Y1j}}$	−12.37	−14.31	3.97	−12.25		
$\overline{K_{Y2j}}$	−13.60	−14.10	−20.28	−13.72		
$\overline{K_{Y3j}}$	−18.10	−15.66	−27.76	−18.10		
R_{Yj}	5.73	1.56	31.73	5.85		
Important order		$C > A > B$				
K_{Z1j}	74.09	66.73	4.82	66.86		
K_{Z2j}	65.69	69.99	108.77	69.85		
K_{Z3j}	59.34	62.40	85.53	70.37		
$\overline{K_{Z1j}}$	24.70	22.24	1.61	22.29		
$\overline{K_{Z2j}}$	21.90	23.33	36.26	23.28		
$\overline{K_{Z3j}}$	19.78	20.80	28.51	23.46		
R_{Zj}	4.92	2.53	34.65	1.17		
Important order		$C > A > B$				

Table 5. The analysis of the variance of the conducted tests' results.

Test index	Test factors	Sum of squares	Degree freedom	Mean square	F Value	Significance level
The slip ratio of inside crawler δ_Y [%]	Calibration model	1709.326	6	284.888	10.257	0.091
	Intercept	1942.459	1	1942.459	69.937	0.014
	A	54.574	2	27.287	0.982	0.504
	B	4.320	2	2.160	0.078	0.928
	C	1650.433	2	825.216	29.712	0.033
	error	55.548	2	27.774		
	Total	3707.333	9			
The slip ratio of outside crawler δ_Z [%]	Calibration model	2030.582	6	338.430	55.923	0.018
	Intercept	4405.419	1	4405.419	727.959	0.001
	A	36.494	2	18.247	3.015	0.249
	B	9.665	2	4.832	0.799	0.556
	C	1984.423	2	992.211	163.955	0.006
	Error	12.103	2	6.052		
	Total	6448.104	9			

The results in Tables 4 and 5 show that the important order of the influence factors on the sliding ratio of the crawler is as follows: the steering radius $C >$ the pavement condition $A >$ the speed B. Among them, the steering radius has a significant influence on the slip ratio of inside crawler, and has an extremely significant effect on the slip ratio of outside crawler. Tables 4 and 5 show that the inside crawler of the chassis is at low speed, and the slip would occur generally; the slip ratio is less than zero. With the increase of the relative humidity of the pavement, the slip ratio of inside crawler rises. This is due to the increase of the pavement humidity, the slip degree of the crawler is larger, which lead to the increase of the slip ratio of inside crawler. With the increasing of the speed, the slip ratio of inside crawler has a trend of decreasing first and then increasing; when the speed is about 0.70 m/s, the slip ratio of the inside crawler is at a minimum. With the continuous increase of the steering radius, the slip ratio of the inside crawler decreases gradually to the negative slip ratio and then increases gradually. This is due to the fact that the smaller the steering radius, the larger the sliding of the inside crawler is, and the chassis also moves laterally in the steering, which affects the size of the slip ratio. The outside crawler of the chassis is at high speed, and the slip generally occurs, and the slip ratio is more than zero. With the increase of the relative humidity of the pavement, the slip ratio of the outside crawler showed a trend of decline. With the acceleration of

Fig. 5. The steering drive torque on different pavements: a) the unilateral steering on dry cement road, b) the free steering on dry cement road, c) the unilateral steering in the fields, d) the free steering in the fields.

the speed, the slip ratio of the outside crawler has a trend of increasing first and then decreasing. The slip ratio of the outside crawler is at a maximum when the speed is about 0.70 m/s. However, with the continuous increase of the steering ratio, the slip ratio of the outside crawler increases first and then decreases. When the speed is about 0.36 m, the slip ratio of the outside crawler is at a maximum.

6. Conclusion

Using the multi-body dynamics simulation software RecurDyn, the dynamic model of the chassis is established. The dynamic simulation analysis of the steering process of chassis riding on the sandy loam and clay pavements is conducted. The results show that the steering on the sandy loam ground is harder to control than on the clay ground. The resistance torque of pivot steering for the chassis is at maximum, and then the driving torque of inside and outside driver is roughly equal to approx. 552 $\mathrm{N} \cdot \mathrm{m}$. In the pivot steering, the operation is flexible with short steering time. The steering body only needs seven seconds to rotate

360°, and the simulation results are consistent with the theoretical calculation and analysis. The test results showed that the important order of the influence factors for the sliding ratio of the chassis on both sides is such that the steering radius $C >$ the pavement condition $A >$ the speed B. The steering radius has a significant effect on the slip ration of the inside crawler, and has an extremely significant effect on the slip ration of the outside crawler. With the increase of the relative humidity of the pavement, the slip ratio of the inside crawler shows a rising trend. With the acceleration of the speed, the slip ratio of the inside crawler shows a trend of decreasing first and then increases; the slip ratio of the inside crawler is at a minimum when the speed is about 0.70 m/s. With the constant increase of the steering radius, the slip ratio of the inside crawler decreases gradually and then increases. The slippage rate of the outside crawler displays a decreasing trend with the increase of relative humidity. With the acceleration of the speed, the slippage rate shows a trend of increasing first and then decreases. The slippage rate of the outside crawler is at a maximum when the speed is about 0.70 m/s. With the increase of steering radius, the slippage rate increases first and then decreases; the slippage rate of the outside crawler is at a maximum when the steering radius is about 0.36 m.

Acknowledgments

The study was supported by the Key Laboratory of Modern Agricultural Equipment, Ministry of Agriculture, P.R. China (201602002), Excellent Talents Training Program by the Ministry of Education (gxfx2017125), and planning project of Chuzhou University (2015GH43).

References

1. Zheng R.G., *Analysis of application performance of crawler chassis in agricultural production* [in Chinese], Agricultural Use and Repair, (6): 15, 2004.
2. Chi Y., Wang H.T., Shi D.D., Zhang R., *Research on steering power ratio for skid-steering with small radius of tracked vehicles adopting differential steering mechanism* [in Chinese], Transactions of the Chinese Society of Agricultural Engineering (Transactions of the CSAE), **45**(12): 112–118, 2014.
3. Li S., Gang X.Y., Yu H.X., *A 3-DOF dynamical model and steering simulation for a rigid vehicle* [in Chinese], Machinery Design & Manufacture, (3): 260–264, 2015.
4. Yang L., Ma B., Li H.Y. *et al.*, *Performance simulation of hydrostatic drive tracked vehicles differential and independent steering* [in Chinese], China Mechanical Engineering, (3): 624–629, 2010.
5. Al-Milli S., Seneviratne L.D., Althoefer K., *Track-terrain modeling and traversability prediction for tracked vehicles on soft terrain*, Journal of Terramechanics, **47**(3): 151–160, 2010.

6. Ding L., Gao H.B., Deng Z.Q., Li Y., Liu G., *New perspective on characterizing pressure-sinkage relationship of terrains for estimating interaction mechanics*, Journal of Terramechanics, **52**: 57–76, 2014.
7. Bekker M.G., *Introduction to Vehicle System – Ground* [M], Mechanical Industry Press, Beijing, 1978.
8. Chi Y., Zhang R.G., Ren J., Li H., Wang Y., *Steering power ratio affected by soil sinkage with differential steering in tracked vehicle* [in Chinese], Transactions of the Chinese Society of Agricultural Engineering (Transactions of the CSAE), **32**(17): 62–68, 2016.
9. Sandu C., Worley M.E., Morgan J.P., *Experimental study on the contact patches pressure and sinkage of a lightweight vehicle on sand*, Journal of Terramechanics, **47**: 343–359, 2010.
10. Yang L., Ma B., Li H.Y. *et al.*, *Research hydraulic drive armored tracked vehicle steering characteristic simulation*, Ordnance Journal, (6): 663–668, 2010.
11. Lu J.J., Wei L.S., Zhao T.S., *Based RecurDyn Slip on tracked vehicle acceleration performance impact study*, System Simulation Technology, (7): 139–143, 2007.
12. Shabana A.A., Sany J.R., *A survey of rail vehicle track simulations and flexible multibody dynamics*, Nonlinear Dynamics, **26**(2): 179–212, 2001.
13. Cheng J.W., Gao L.H., Wang L.X. *et al.*, *Based on the high-speed turn under slippery conditions Tracked Vehicle*, Vehicle and Power Technology, (1): 44–48, 2006.
14. Li X.Y., Zhang Y., Hu J.B., Yuan S.H., *Skid-steering resistance characteristics of wheeled vehicle*, Acta Armamentarii, **32**(12): 1433–1438, 2011.
15. Lu J.J., Wei L.S., Zhao T.S., *Based on the tracked vehicle speed RecurDyn steering dynamics simulation study*, Modern Machinery, (1): 10–12, 2008.
16. Chen S.Y., Sun F.C., *Study on modeling and turning performances for electric drive tracked vehicle propulsion system*, Journal of System Simulation, **18**(10): 2815–2818, 2006.
17. Liu K., Ayers P., Howard H., Anderson A., *Influence of turning radius on wheeled military vehicle induced rut formation*, Journal of Terramechanics, **46**(2): 49–55, 2009.
18. Wang J., Wei L.S., Lan X.P., *Modeling and simulation of driver-tracked vehicle-road system*, Computer Integrated Manufacturing Systems (CIMS), (9): 108–111, 2003.
19. Ma X.G., Chen Y.Y. *et al.*, *Based on the multi-body dynamics simulation analysis of the tracked vehicle steering performance*, Mechanical Design, **29**(6): 52–56, 2012.
20. Fang S.S., Lu Z.X, Wang Z.C. *et al.*, *Design and prototype performance experiments of steering-by-wire hydraulic pressure system of tractor* [in Chinese], Transactions of the Chinese Society of Agricultural Engineering (Transactions of the CSAE), **33**(10): 86–93, 2017.
21. Wen A.M., Lu Z.X., Wu J.G., *Experiment and analysis of full hydraulic steering characteristics* [in Chinese], Journal of Chinese Agricultural Mechanization, **35**(5): 122–127, 2014.
22. Long J.Q., *Research on the test way and evaluation indexes of the vehicle's steering stability* [in Chinese], Popular Science & Technology, **17**(8): 70–71, 2015.

Received August 21, 2017; accepted version July 6, 2018.